Synchrotron Analysis of Human Organ Tissue Exposed to Implant Material

Ilona Swiatkowska[1], J. Fred W. Mosselmans[2], Tina Geraki[2], Cody C. Wyles[3], Joseph J. Maleszewski[3], Johann Henckel[4], Barry Sampson[5], Dominic B. Potter[6], Ibtisam Osman[5], Robert T. Trousdale[3], Alister J. Hart[1,4]

[1]Institute of Orthopaedics and Musculoskeletal Science, University College London, HA7 4LP Stanmore, UK
[2]Diamond Light Source, Harwell Science and Innovation Campus, OX11 0DE Didcot, UK
[3]Mayo Clinic, 200 1st Street SW, Rochester, MN, USA
[4]Royal National Orthopaedic Hospital, Stanmore, HA7 4LP Stanmore, UK
[5]Trace Element Laboratory, Department of Clinical Chemistry, Charing Cross Hospital, Imperial College NHS Healthcare Trust, W6 8RF London, UK
[6]Departament of Chemistry, University College London, WC1H 0AJ London, UK
Correspondence and requests for materials should be addressed to I.S. (email: ilona.swiatkowska.10@ucl.ac.uk, phone number: 0208 426 3412)

ABSTRACT

Background: Orthopaedic implants made of cobalt-chromium alloy undergo wear and corrosion that can lead to deposition of cobalt and chromium in vital organs. Elevated cardiac tissue cobalt levels are associated with myocardial injury while chromium is a well-established genotoxin. Though metal composition of tissues surrounding hip implants has been established, few investigators attempted to characterize the metal deposits in systemic tissues of total joint arthroplasty patients.

Methods: We report the first use of micro-X-ray fluorescence coupled with micro-X-ray absorption spectroscopy to probe distribution and chemical form of cobalt, chromium and titanium in postmortem samples of splenic, hepatic and cardiac tissue of patients with metal-on-polyethylene hip implants (n=5).

Results: Majority of the cobalt was in the 2+ oxidation state, while titanium was present exclusively as titanium dioxide, in either rutile or anatase crystal structure. Chromium was found in a range of forms including a highly oxidised, carcinogenic species (CrV/VI), which has never been identified in human tissue before.

Conclusions: Carcinogenic forms of chromium might arise in vital organs of total joint arthroplasty patients. Further studies are warranted with patients with metal-on-metal

implants, which tend to have an increased release of cobalt and chromium compared to metal-on-polyethylene hips.

1. INTRODUCTION

Orthopaedic implants made of cobalt-chromium(CoCr) alloy undergo wear and corrosion with release of particulate and soluble debris into the surrounding tissue and blood[1]. Elevated blood cobalt(Co) has been linked to neurological complaints, cardiomyopathy and hypothyroidism in some patients[2], while Cr is associated with nephrotoxicity[3] and carcinogenesis[4]. Deposition of metal degradation products in vital organs can lead to tissue damage and, in extreme cases, death[5–8]. Titanium(Ti) may also have a significant potential for eliciting a pathologic response in tissues[9,10]. Millions of patients worldwide who received metal-containing prostheses might be at an increased risk of widespread systemic toxicity and cancer.

In the body, implant-derived cobalt can be found in its metallic(Co^{0}) or divalent(Co^{II}) state- the latter being the primary toxic form. On the other hand, chromium exists in three predominant states: metallic(Cr^{0}), trivalent(Cr^{III}) or hexavalent(Cr^{VI}). While Cr^{III} is only mildly toxic, Cr^{VI} compounds are potent human carcinogens[11]. It is unclear whether implants release Cr^{VI}, with some reports supporting the idea[12,13] and others opposing it[14,15]. Synchrotron analysis of tissue samples from around metal implants revealed an abundance of Cr^{III} phosphate($CrPO_4$) and Cr^{III} oxide(Cr_2O_3), but no evidence of Cr^{VI}[16,17]. Organs of total joint arthroplasty(TJA) patients have also been probed for metal content[18–21], but chemical speciation of the metal deposits was only investigated in one case[22]. Herein, a systematic approach involving optical microscopy, laser ablation inductively coupled plasma mass spectrometry, micro-X-ray fluorescence and micro-X-ray absorption spectroscopy was employed to study: 1) distribution of Co, Cr and Ti in organs of TJA

patients and 2) chemical speciation of the metal deposits. Detailed characterization of the physicochemical properties of implant-derived debris is crucial to assess the possible long-term systemic implications posed by medical biomaterials, and to identify patient groups that might be at an increased risk of adverse effects.

2. MATERIALS AND METHODS

2.1. Tissue samples

Consented tissues were obtained from the Mayo Clinic Tissue Registry (1990–2011) and used with approval of the Mayo Clinic Institutional Review Board (IRB 16-005246). Samples of left ventricular (n=5), hepatic (n=5) and splenic (n=3) tissue were acquired post-mortem from 5 MoP patients. The patients' clinical data and implant composition is summarized in Table 1. The patients died from a variety of conditions, though not thought to be related to the joint prosthesis. The use of dietary supplements had not been documented in this group.

Table 1. Implant materials and the patients' clinical data.

#	Gender, age at death	Implant materials[a]	Cumulative implant years	Cardiac Co, Cr (μg/g dry tissue)	Cause of death	Necropsy findings
1	M,79	2 THA- 32 mm CoCr head, CoCr stem, cemented, Ti acetabular cup; 1 TKA	28.6	0.91, 0.30	Probable sepsis, diabetes mellitus (clinical), reactive hyper cellular bone marrow, mild	Cardiomegaly, interstitial fibrosis
2	M,82	2 THA- 28 and 32 mm CoCr heads, Ti stems, uncemented, CoCr modular neck, Ti acetabular cup; 2 TKA	52.3	0.59, 0.08	Acute bronchopneumonia	Cardiomegaly, interstitial fibrosis
3	M,49	1 THA- 36 mm CoCr head, CoCr	1.7	0.35, 0.06	Brain death, acute subdural hematoma,	Cardiomegaly

		stem, uncemented, CoCr modular neck, Ti acetabular cup			seizure, seizure disorder, papillary thyroid cancer	
4	F,87	1 THA- 36 mm CoCr head, CoCr stem, uncemented, Ti acetabular cup	5.7	0.34, 0.14	1. Acute/ongoing myocardial infarction secondary to atherosclerotic ischemic heart disease, coronary atherosclerosis; 2. Anemia, diabetes mellitus (type II)	Interstitial fibrosis
5	F,79	2 THA- 28 and 32 mm CoCr heads, CoCr stem, cemented, CoCr modular neck, Ti acetabular cup	17.9	0.31, 0.16	1. Subdural hematoma, fall at home; 2. Remote heart transplantation (1992), end stage renal disease	Cardiomegaly

[a]All CoCr components were made of ASTM F75 alloy with cobalt content of 60-65 % and chromium content of 26-30 %.

The tissue samples were cut using polytetrafluoroethylene (PTFE)-coated instruments to reduce the risk of potential metal contamination. The specimens were fixed in 10% neutral buffered formalin and processed in paraffin wax. Three adjacent sections were cut from each paraffin block (Figure 1). H&E stained sections were investigated under optical microscope to look for visible metal debris and associated tissue irregularities, while laser ablation inductively coupled plasma mass spectrometry(ICP-MS) helped us to map areas of increased Co and Cr concentration in the tissue. The two techniques guided our choice of tissue areas for the more detailed synchrotron X-ray analysis. Cardiac Co and Cr content was established by ICP-MS as previously described[23].

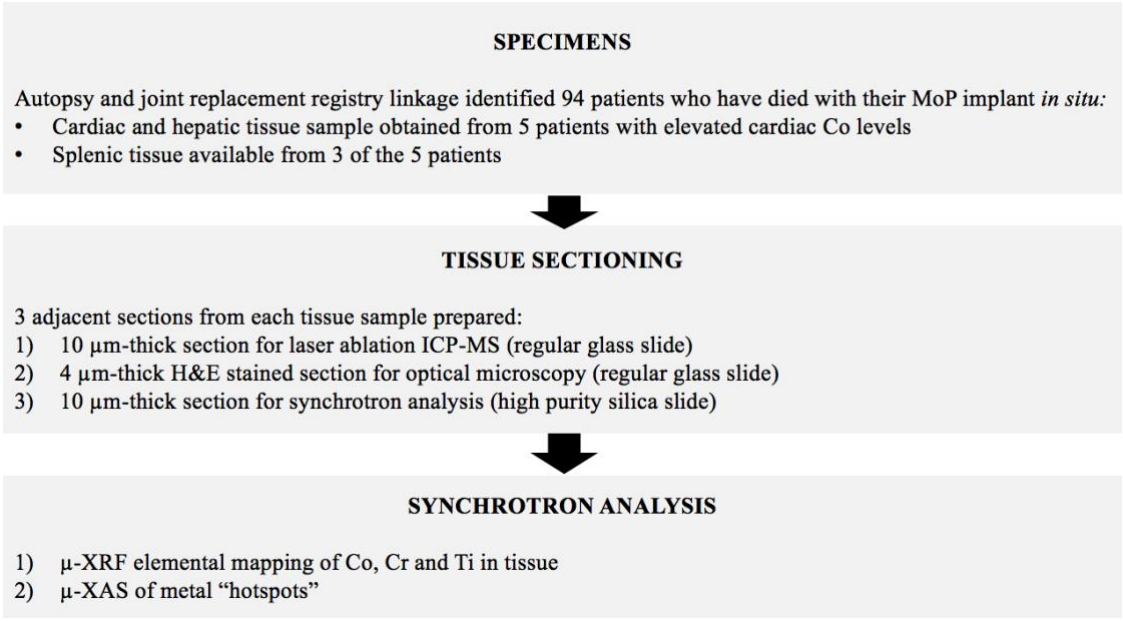

Figure 1. Schematic diagram of study design.

2.2. Laser ablation ICP-MS

A quadrupole-based inductively coupled plasma mass spectrometer (ICP-MS, Agilent 7900, Agilent, Stockport, UK) coupled to a laser ablation system (New Wave UP213, ESI, Huntingdon, UK) was used to study distribution of Co and Cr in samples of cardiac, hepatic and splenic tissue. Laser ablation of biological tissue was performed using a focused laser beam in the scanning mode (Table A.1) with a series of lines about 2-3000 µm long and with a total of 40-60 lines giving a total ablated area of up to 3000x3000 µm (the exact size varied between samples). Other elements were measured to provide additional information about the tissues (Table A.2) and will be reported in a separate publication. The total time for all of the isotopes corresponded to a distance of 25 µm so that each sample represented an area of 25x25 µm. The ablated material was transported by helium gas (as carrier gas) into the inductively coupled plasma. The ions formed in the process were extracted in the ultrahigh vacuum mass spectrometer via a differential pumped interface, separated in the quadrupole mass analyzer according to their mass-to-charge ratios and detected by an ion detector (Table A.3). Data was exported from the ICP-MS as csv files and imported into the program

Origin2017 (OriginLab, Northampton, Massachusetts, USA) to generate distribution maps of the isotopes.

2.3. Synchrotron techniques

The tissue samples, which were mounted on high purity silica slides, were dewaxed by sequential immersion in xylene and alcohol. The synchrotron work was carried out on the microfocus spectroscopy beamline (I18) at Diamond Light Source, Harwell Science and Innovation Campus (Didcot, UK)[24]. We performed two types of experiments: micro X-ray fluorescence(μ-XRF) elemental mapping and microfocus X-ray absorption spectroscopy(μ-XAS) with a typical beam profile of 3 x 3 μm, providing a resolution at a length scale similar to that of individual cells.

2.3.1. μ-XRF

Large tissue areas (typically 3000x2000 μm) were mapped at room temperature using an incident X-ray beam of 8.5 keV and a 4 element Si drift Vortex ME4 detector (Hitachi Hi-Technologies Science America) with Xspress-3 processing electronics, at fixed sample-detector distance (75 mm). 1-3 areas per tissue section we scanned to increase the probability of finding metal deposits. The resultant two-dimensional elemental maps displayed "hotspots" of increased metal concentration. The initial fluorescence maps were collected using a slightly defocused beam with a 20 μm step in each direction. These regions of interest were subsequently scanned with a 3-5 μm step to locate metal deposits to within a few microns. Raw data was processed using PyMCA software[25]. The representative spots in each XRF map were quantified for relative Co/Cr content in the same software.

2.3.2. μ-XAS

μ-XAS spectra of the Co, Cr and Ti "hotspots" were acquired in fluorescence mode due to the low concentration of metal in the tissue samples. The X-ray absorption near-edge structure(XANES) part of the spectrum (from 30 eV below to about 50 eV above the absorption edge) was used to determine the oxidation state of the metal. Information on atoms surrounding the X-ray absorbing atom was gleaned from both comparisons of the XANES with standard spectra and, in one case, the extended X-ray absorption fine structure(EXAFS) portion of the spectrum, which, although short, was of sufficient quality to analyse. The majority of μ-XAS measurements were done in duplicate to improve data quality and investigate possible beam damage to the sample. Spectra were also collected in transmission mode from Co, Cr and Ti metal foils, to serve for energy calibration. Reference standards were compared with experimental measurements using Athena software in order to determine speciation[26]. EXAFS data was analysed using the Artemis program in a standard manner[26].

3. RESULTS

3.1. ICP-MS

Median cardiac Co and Cr level was 0.35 (range, 0.31-0.91) and 0.14 (range, 0.06-0.30) μg/g dry tissue, respectively, and did not differ significantly based on femoral stem material (CoCr vs Ti) or between fixation methods (cemented vs uncemented). The median cardiac Co load was mildly elevated (normal: 0.06 μg/g[27]).

3.2. Optical microscopy

Preliminary investigation of H&E stained tissue by conventional optical microscopy indicated presence of fine particulate matter in all three spleen samples, and in Patient 5 liver,

but not in the remaining organs. Assuming that the tissue samples were representative of the particle burden of the organ as a whole, the absence of visible particles in most tissue sections suggests that they were too small to be seen (<1 µm), or had already corroded and dissolved.

3.3. Elemental mapping of metals in tissue

In total, 25 areas from 5 cardiac, 4 hepatic and 3 splenic tissue samples were mapped. Co and Cr were highly co-localised in all splenic XRF maps (n=8). A small number of spots with co-localised Co and Cr were identified in hepatic tissue of Patients 1, 4 and 5, and in cardiac tissue of Patient 5. We also recognized a few spots with co-localised Cr and Ti and two with co-localised Co and Ti. In general, splenic tissue displayed the highest counts of metal in the XRF maps, followed by hepatic tissue and cardiac tissue. When the brightest spot in each XRF map was probed for relative Co and Cr content, the Co/Cr ratio ranged from 2.4 to 0.02 in Patient 1 spleen and Patient 2 heart, respectively. Splenic tissue displayed the highest Cr/Cr ratio, followed by hepatic and cardiac tissue.

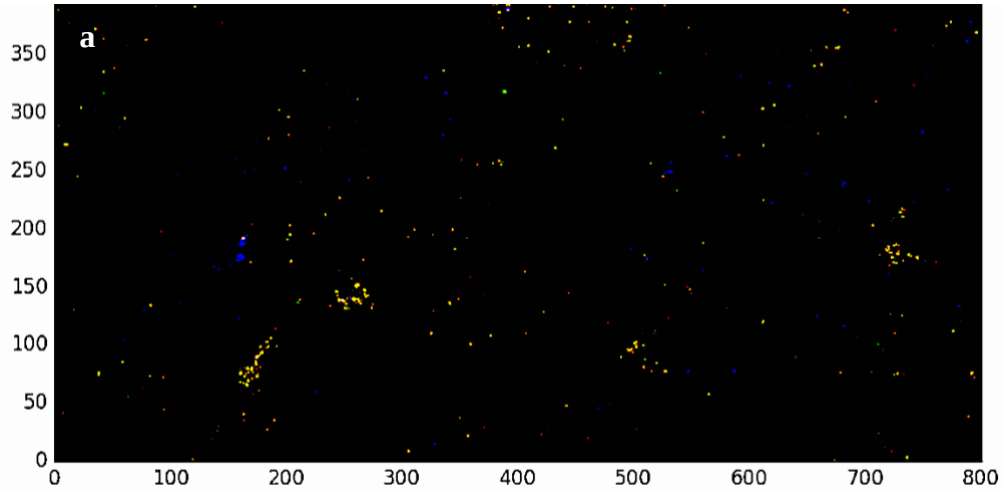

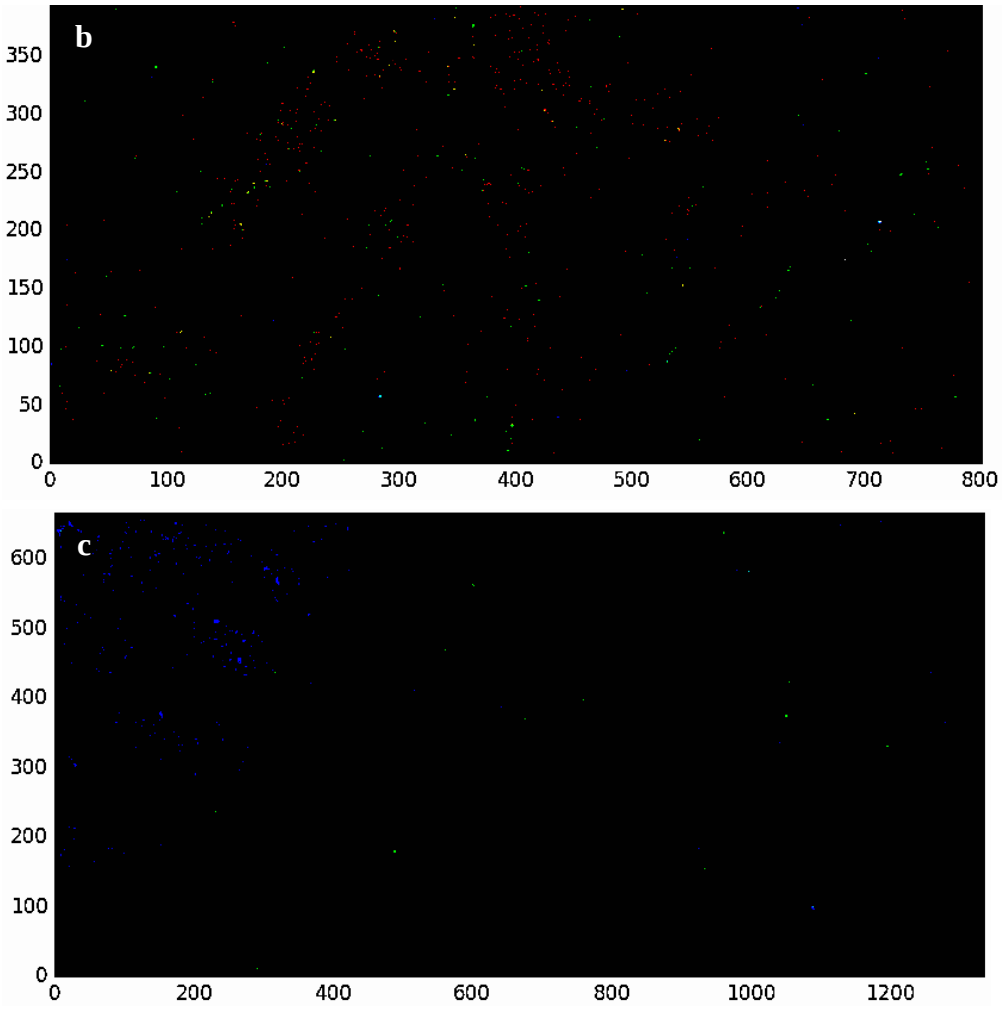

Figure 2. Representative XRF maps of a) spleen tissue (2x4 mm, 5 µm step size), b) liver tissue (2x4 mm, 5 µm step size) and c) left ventricular tissue (2x4 mm, 3 µm step size) showing Co (red), Cr (green) and Ti (blue) "hotspots". Yellow spots indicate co-localised Co and Cr. In each image, image brightness and contrast have been adjusted to improve visibility of the described features.

3.4. Chemical speciation of metals in tissue

3.4.1. Chromium

Cr K-edge XAS spectra were recorded at 12 separate points from 2 cardiac, 2 hepatic and 3 splenic tissue samples. Four points generated unusable data, likely due to the particle size being too small. Where better quality data was obtained, Cr could be found in either a metallic-like form(Cr^0), in the Cr^{III} form, or in a more highly oxidized state characterized by a sharp pre-edge peak in the XANES spectrum (Figure 3). The latter was identified in all three

organs from Patient 1, as well as in Patient 4 spleen. The spectrum recorded at a Cr hotspot in Patient 2 liver also featured a pre-edge peak, but its profile was different. Since the pre-edge peak "grew" in the duplicate scan, it is likely that the Cr was originally in the trivalent state, but underwent oxidation due to the prolonged X-ray beam exposure (Figure 4b).

In one case only the data was of sufficient quality to warrant EXAFS analysis. For the Patient 1 splenic tissue point, six oxygens could be fitted at a distance of 1.97 Å, suggesting perhaps a hydrated Cr^{III} species, i.e. $Cr^{III}(H_2O)_6$ (Figure A.1).

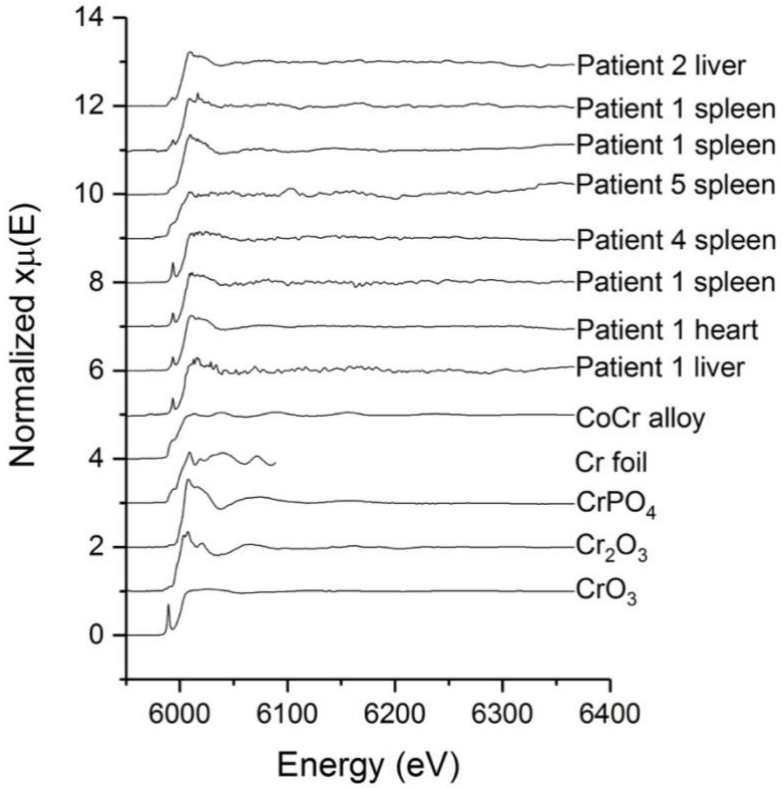

Figure 3. Stacked XANES spectra recorded at the Cr edge of eight tissue "hotspots" along with spectra for six chemical standards. The top three traces are Cr^{III}-like, fourth one resembles metallic-like Cr, while the bottom four spectra resemble the Cr^{VI} standard.

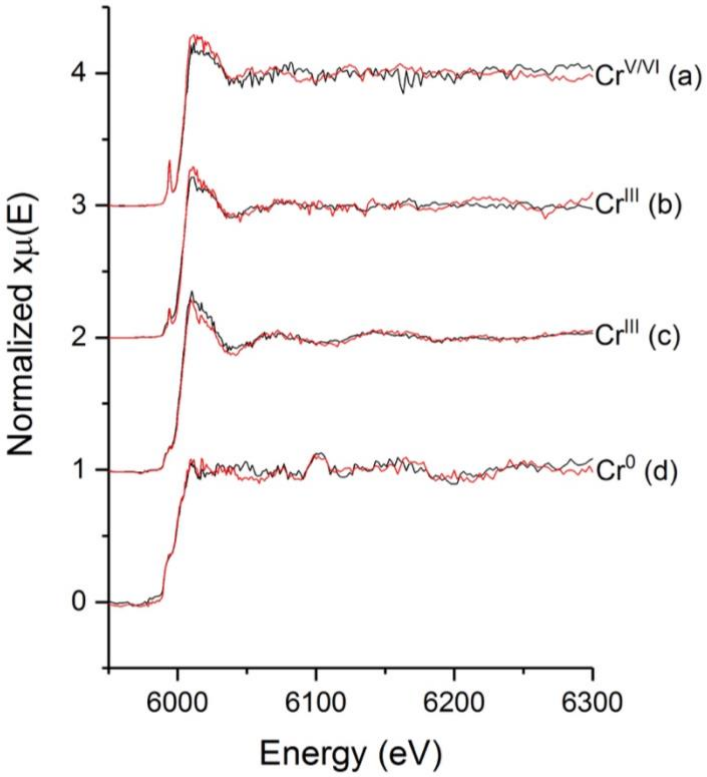

Figure 4. Replicate XANES spectra of the different Cr forms found in the tissue samples. In each case, the duplicate scan (red line) was performed 20 minutes after the initial one (black line).

3.4.2. Cobalt

We recorded Co K-edge XAS spectra at 9 separate points from 1 cardiac, 1 hepatic and 3 splenic tissue samples. Absorption edge was not observed in three cases, indicating that the Co concentration was below the detection limit. In the remaining cases the low signal-to-noise ratio complicated analysis. Overall, most of the spectra resembled the Co^{II} state, with two exceptions from Patient 1 spleen (Figure 5). At those two points, the Co appeared to have been originally in the metallic form (either pure metal or CoCr alloy), which was oxidized due to X-ray beam exposure in the duplicate scan. Similar effect was observed in previous work investigating Co speciation in periprosthetic tissue[28].

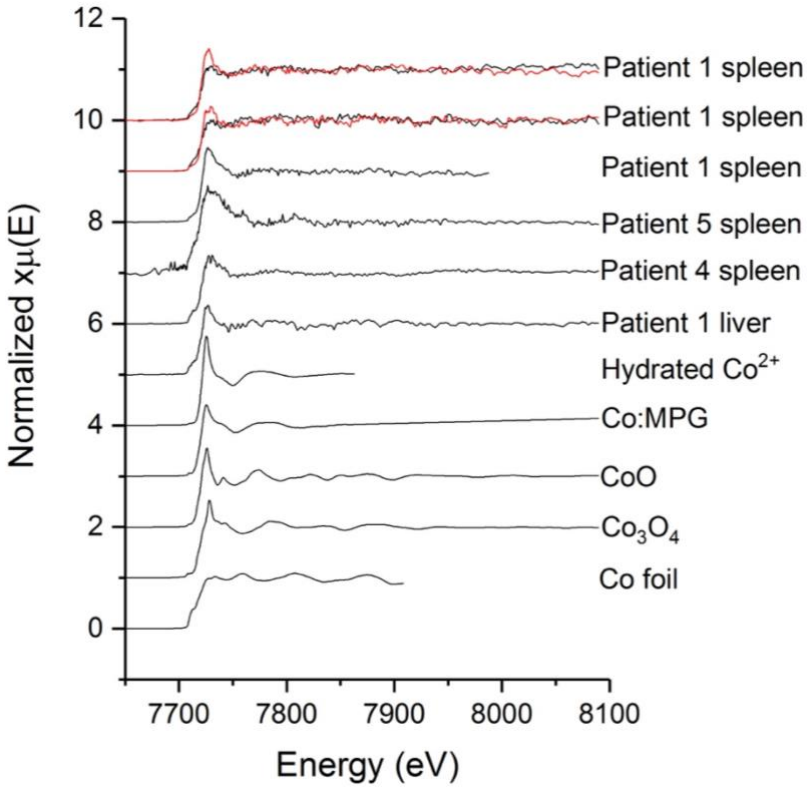

Figure 5. Stacked XANES spectra from Co "hotspots" along with chemical standards. The top two traces correspond to metallic-like Co that was oxidized by the beam in the duplicate scan (red line). The remaining spectra resemble the Co^{II} standard. MPG- N-(2-mercaptopropionyl)glycine.

3.4.3. Titanium

The pre-edge features found in all the Ti K-edge XANES spectra were consistent with those of titanium dioxide(TiO_2). Rutile was the predominant crystal structure, with anatase present in 4 out of the 13 points scanned (Figure 6).

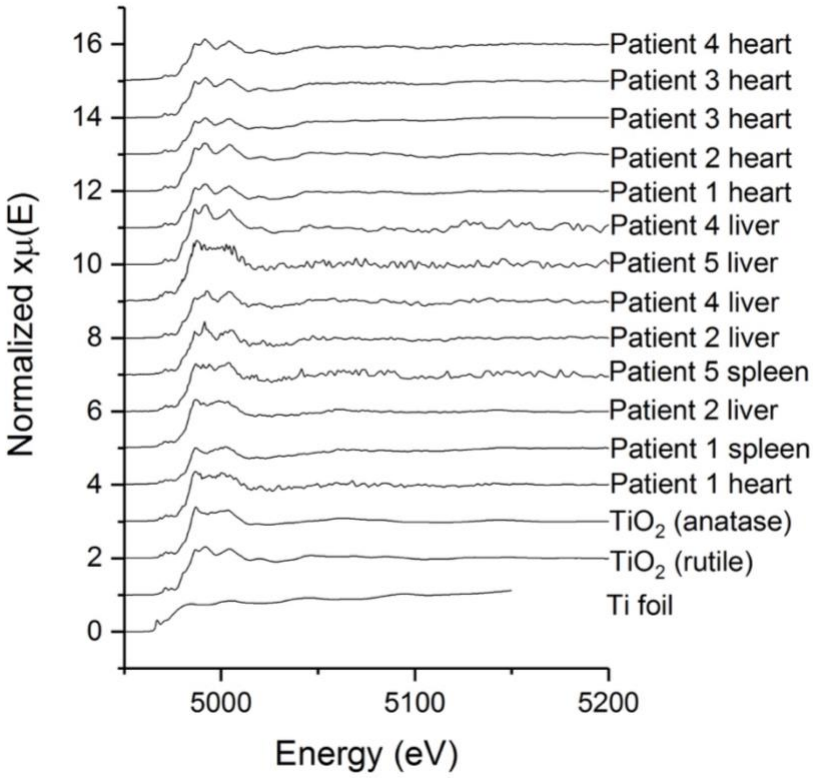

Figure 6. Stacked XANES spectra from Ti "hotspots" along with chemical standards. All spectra are representative of TiO_2- the top nine traces are rutile-like while the bottom four resemble anatase.

4. DISCUSSION

Periprosthetic tissues surrounding metal-on-metal(MoM) and metal-on-polyethylene(MoP) implants have been found to contain metallic CoCr particles, $CrPO_4$ and Cr_2O_3 but no detectable Cr^{VI}[28–32]. Data on Co and Cr speciation in systemic tissues of TJA patients is scarce. To date, only one study investigated the chemical form of Co and Cr liver deposits in a patient with extremely elevated blood metals from a failed hip prosthesis[22]. The authors found highly co-localized Co and Cr metallic particles in hepatic macrophages, with no sign of Cr^{VI}. In the current study, we explored the metal composition of splenic, hepatic and cardiac tissue samples from 5 TJA patients and, for the first time, identified a chromium species more highly oxidized than Cr^{III} in human tissue.

4.1. Meal release and systemic dissemination

CoCr alloy is considered highly biocompatible due to the spontaneous formation of a chromium oxide-rich passivation layer, which protects the underlying metal from corrosion[33]. However, once the alloy is implanted, a combination of wear and corrosion forces induces selective fractures of the protective film. CoCr alloy particles and corrosion products are phagocytosed by tissue-resident macrophages and transported around the body in endosomal compartments. The acidic pH of the endosome causes the particles to release Cr and Co ions with different oxidation states, out of which Co^{II}, Cr^{III} and Cr^{VI} are the most stable[1]. While Cr^{III} is considered relatively benign, Cr^{VI} is an established human carcinogen as it enters cells more easily[34,35]. Deposition of Cr, particularly in the Cr^{VI} form, in vital organs is of concern due to the carcinogenic nature of the metal. The extent to which Co accumulates in the organs is also of interest. Elevated cardiac Co loads have been linked to cardiac dysfunction and several cases of fatal cardiomyopathy (Table A.4). It is thought that Co exerts its toxic effect via interference with myocardial energy metabolism. Pyruvate and lactate accumulation in the mitochondria increases osmotic pressure, resulting in oedema and structural disruption[36]. In our series, even though the concentration of Co in the heart was only mildly increased, 80% of the patients exhibited cardiomegaly and 60% of cases displayed severe interstitial fibrosis.

4.2. Analysis of XRF maps

Dissemination of metal debris to the liver, spleen and heart is a common occurrence in TKA and THA patients[18,21]. In iron(Fe) loading states the deposition of Fe occurs primarily in the liver, followed by other organs including the heart[22]. A similar pattern may be seen with Co and Cr. In the current study, data on splenic and hepatic Co/Cr concentration was unavailable, so we were unable to draw comparisons with the cardiac load. However, the relative decrease in the number and intensity of metal “hotspots” in the cardiac maps

compared to splenic maps suggests progressive particle processing during systemic transport, and is consistent with the notion that dissemination of debris form a hip implant occurs predominantly via lymphatic spread[37]. The Co/Cr ratio in tissue decreased with increasing distance from the implant in all three patients from which cardiac, hepatic and splenic tissue samples were available for comparison. For example, while the Co/Cr ratio in Patient 1 spleen was 2.4, i.e. similar to that in bulk alloy, in the liver it decreased to 1, and further down to 0.3 in the heart. Co is more soluble and corrodes faster than Cr, which might lead to selective "leaching" of Co from metallic particles and to its enrichment in organs. In contrast, the relatively insoluble Cr tends to accumulate in the hip joint[38]. The spots in which Co and Cr were co-localised could have been particles of CoCr alloy. However, it was impossible to discern whether the metals were chemically bound together or if they were separate metal particles that were near each other in the tissue. Co-localisation of Ti with Co or Cr likely occurred inside phagocytic cells.

The titanium could have originated from the acetabular shell featured in all of the hip implants (and the femoral stem in Patient 2). However, it is likely that external sources were the main contributor to the total tissue Ti load. TiO_2 is a common additive in many food and personal care products[39], as well as being present in ambient air. Biodistribution experiments showed that oral intake of TiO_2 nanoparticles could lead to their deposition in the spleen and the liver and result in accumulation in tissues upon repeated exposure[40].

4.3. Analysis of Cr XAS spectra

4.3.1. Chemical speciation

Chromium was present in three different oxidation states in the specimens studied. Much of the data resembled metallic Cr and Cr^{III} compounds, which have been identified in periprosthetic samples before[16,28,32]. However, we are the first to report on a chromium

species more highly oxidized than Cr^{III} in human tissue. Cr XANES spectra taken at four different points in the tissue specimens featured a sharp pre-edge absorbance, assigned to a symmetry-forbidden 1s→3d electronic transition, which unambiguously confirms the presence of high oxidation states of Cr i.e. $Cr^{IV/V/VI}$[41]. The exact chemical form of the complexes could not be elucidated. The XANES spectra did not match any of the available chemical standards, nor that of Cr^{VI}-glutathione complex (likely intermediate formed during the cellular metabolism of Cr^{VI})[42]. The traces bore the most resemblance to that of Na_2CrO_4/Cr_2O_3 mixture described by Bajt et al[43]. It is well-established that the height of the pre-edge absorbance can offer quantitative information on the proportion of Cr^{VI} in a mixture of Cr^{III} and Cr^{VI} oxides[43–45]. Since in all four cases the pre-edge band was only about a third as intense as that of pure Cr^{VI} standard, it is possible that the spectra we observed correspond to a 30-40% mixture of Cr^{III} and Cr^{VI} oxides. Notably, XANES spectrum of a Cr^{V}-carbohydrato intermediate, that is thought to form in biological systems exposed to Cr^{VI}, featured a pre-edge peak of similar intensity[46]. However, it is much less probable that our spectra correspond to Cr^{V} species. Even though certain carbohydrates can stabilize the reactive Cr^{V} intermediate in vivo[47], the resultant complexes would be expected to undergo rapid photodecomposition and this was not observed in our case. The intensity of the pre-edge peak or the edge position did not change when we repeated the XANES scan at the same point, indicating a stability of the $Cr^{V/VI}$ complex towards photoreduction and photooxidation (Figure 4a). This is in contrast to the $Cr^{V/VI}$ species described by Wu et al, which was recorded in Cr^{III}-treated rat adipocytes[41]. The authors noted a decrease in the pre-edge absorbance intensity between two sequential XANES scans at the same spot (approx. 0.5 to 0.3 normalised absorbance). A probable explanation for the difference between our findings and those of Wu et al is that the $Cr^{V/VI}$ species produced as a result of intracellular oxidation of Cr^{III} supplements is different to that of prosthetic-derived

Cr^{III}. We can exclude that the species is a Cr^{IV} complex, as those are notoriously unstable[42]. Besides, the energies of pre-edge absorbance observed in model Cr^{IV} complexes[48] are considerably different to those recorded in the current study.

4.3.2. Origin

It is unlikely that the $Cr^{V/VI}$ species originated directly from the orthopaedic implant. The high sequestering and reducing capacity of the blood means that any Cr^{VI} released as a result of wear or corrosion would have been reduced to Cr^{III} before it had the chance to reach organ tissue[49]. Re-oxidation of Cr^{III} to Cr^{VI} under physiologically relevant conditions is, however, possible[50]. Although cellular environments are generally reducing[51], significant local concentrations of strong oxidants are formed during normal cell signaling and, even more so, under pathological conditions[52,53]. In fact, evidence is mounting that insulin-enhancing activity of Cr^{III} supplements is mediated by in vivo oxidation to $Cr^{V/VI}$[54]. Elevated levels of biological oxidants in the blood of diabetics might play a role in facilitating said process. Interestingly, both patients in which the highly oxidized Cr species were recorded were diabetic. It is conceivable that the increased production of reactive oxygen species commonly associated with diabetes[55] could have encouraged oxidation of implant-derived Cr^{III} to higher valence states.

4.4. Analysis of Co XANES spectra

Previous studies investigating chemical composition of tissues surrounding MoM and MoP hip implants reported on the presence of Co^{II} complexed with organic ligands in an octahedral environment (e.g. Co:MPG complex)[16,17,28]. In the current study, most Co XANES spectra resembled Co^{II}, but we were unable to establish the exact chemical form of the metal due to poor data quality.

4.5. Analysis of Ti XANES spectra

Tissues surrounding Ti alloy implants have been found to contain TiO_2 in either anatase, rutile[56] or amorphous form[17]. Our investigation identified TiO_2 in most of the systemic tissue samples. All of the Ti XANES spectra featured small pre-edge peaks that represent transitions to d orbitals in anatase and rutile crystal structures. There was no obvious pattern or trend in the distribution of the two crystal structures in the different organs or patients.

4.6. Study strengths and limitations

Deposition of metal in systemic organs of TJA patients is hard to quantify without an invasive biopsy, meaning that currently available evidence is not always robust. Organ samples obtained at necropsy are ideal specimens for this purpose, however, they are difficult to access. In the current study, we had the unique opportunity to work with cardiac, hepatic and splenic tissue from patients who died with their joint prostheses in situ. From a clinical relevance standpoint, all post-mortem samples are handled in a similar way to ante-mortem samples. They are processed in the same processors, cut on the same microtomes and sampled the same way, which mitigates any artifact based on specimen source. The systematic methodology we employed to study distribution and speciation of metals in the tissue specimens is the main strength of our investigation.

Table 2. Summary of techniques commonly employed to study metal composition of human tissue samples, and the information they can provide.

	Tissue mapping	**Cellular mapping**	**Elemental identification**	**Valency**	**Chemical form**	**Sample preparation**	**Destructive?**
Optical microscopy	+	+	-	-	-	Staining	NO

Laser ablation ICP-MS	+	-	+	-	-	Dewaxing	YES
µ-XRF	+	-	+	-	-	Dewaxing	NO
µ-XAS	-	-	+	+	+	Dewaxing	NO
TEM	-	+	+	+	+	Fixation, dehydration, resin embedding, semithin sectioning, staining	YES
SEM/ EDXA	-	+	+	-	-	Fixation, dehydration, drying, metal coating	YES

TEM- Transmission Electron Microscopy
SEM/EDXA- Scanning Electron Microscopy with Energy Dispersive X-Ray Analysis

Firstly, laser ablation ICP-MS was used to identify metal deposits that, in many cases, were too small to be seen by conventional microscopy. Next, corresponding areas on the adjacent slides were mapped using µ-XRF, which simultaneously provided information on the distribution and relative concentration of the different metals within the sample. The resultant two-dimensional elemental maps displayed "hotspots" of increased Co, Cr or Ti concentration. The "hotspots" were subsequently interrogated with X-rays corresponding to the energy levels of the core shell electrons of the probed element. Spectra generated in this way can be used as fingerprints to identify oxidation state and, if the concentration of the studied metal is high enough, its exact chemical form. The synchrotron techniques we utilized are not destructive, have a low detection limit (hundreds of parts per billion) and enable mapping of large tissue areas followed by repeated analysis of element valency and its nearest atomic neighbours that is widely accepted as precise and accurate. However, if the

concentration of the element of interest is not high enough, XAS is limited to the XANES regime and/or the resulting spectra are very noisy. Another disadvantage of synchrotron technology is its limited availability, which means that the number of specimens that can be analysed will always be much smaller than with other techniques. Due to time constraints, it is also impractical to scan the whole sample. Instead, selected tissue areas are mapped, which might not be representative of the sample as a whole. Mapping of trace metals in tissue can be likened to searching for a needle in a haystack. In our case, the needle was the highly oxidized Cr species, which we identified in as many as 4 different tissue samples from 2 different patients. The replicate Cr XANES scan performed in one of the cases differed only slightly from the original spectrum, with the height of the pre-edge peak and edge energy remaining unchanged. This apparent resistance to photoreduction makes the complex more likely to be a Cr^{VI} species than the inherently less stable Cr^{V}. Comparison with literature standards led us to believe that the spectra most likely corresponded to a mixture of Cr^{III} and Cr^{VI} oxides. However, we cannot prove this. Even though we were unable to confirm the exact chemical speciation of these complexes, our findings are robust and consistent.

4.7. Clinical significance

Exposure to various forms of hexavalent chromium is associated with an elevated incidence of respiratory cancers and other adverse health consequences[35]. Once inside the body, the Cr^{VI} is rapidly reduced to Cr^{III}, which makes it insoluble and restricts its ability to cross cell membranes. The process produces a plethora of noxious species including Cr^{V} and Cr^{IV} intermediates, reactive oxygen species and free radicals that damage cellular proteins, lipids and DNA. This means that Cr^{VI} exerts its toxicological consequences mostly at the point of entry into the organism. The absence of Cr^{VI} from periprosthetic tissue was long regarded as indication that Cr^{VI} generation does not occur during tribocorrosion of CoCr alloy joint

implants. It is also widely held that if Cr^{VI} was to be released, it would be readily reduced and rendered harmless. However, the concept of in vivo re-oxidation of Cr^{III} to Cr^{VI} is still relatively unexplored. Our finding of $Cr^{V/VI}$ in two of the patients uncover the novel possibility that carcinogenic forms of Cr might arise in vital organs of TJA patients. Re-oxidation of Cr^{III} to higher valence states is responsible for the long-term toxicity caused by the exposure to Cr^{VI}, which leads to accumulation of Cr^{III} in cells[57]. Chronically ill patients might be at the highest risk of adverse effects because of the oxidative stress that could provoke oxidation of Cr^{III} to its carcinogenic form. Low concentrations of Cr^{VI} may not pose any serious issues as the built-in detoxification mechanisms prevent the movement of the genotoxin to the cell nucleus. However, if such protective mechanisms are overtaken by large releases of Cr in patients with failing prostheses, or those chronically exposed to the metal, then oxidation of Cr^{III} to Cr^{VI} may present a greater cancer hazard[58]. This issue is especially important because the indications for joint replacements are being extended to younger patients who might be exposed to these materials for 30 years or longer. So far, there is limited evidence for carcinogenic outcomes in TJA patients[59,60], though it could be argued that the follow up time of up to 20 years in the previous studies might not be adequate to detect malignant changes as chromium-produced cancers could take between 20 and 40 years to develop. Of note, even in absence of malignancy, repeated reduction-oxidation cycles and chronic production of reactive species could induce functional failure of the affected organ. Future toxicological studies focusing on MoM patients, and particularly those exhibiting chronic disease states, are warranted to confirm our preliminary findings. This work could ultimately allow clinicians to determine which patients could be at an increased risk of tissue damage and cancer, and enable matching of MoM implants to the most suitable people.

Acknowledgements

The authors would like to thank the Diamond Light Source for the provision of synchrotron beam time and Dr Agata Nyga for help with optical microscopy.

Funding

This work was supported by Gwen Fish Orthopaedic Trust. The funding source did not have involvement in study design, the collection, analysis and interpretation of data, in the writing of the report or in the decision to submit the article for publication.

REFERENCES

[1] B. Scharf, C.C. Clement, V. Zolla, G. Perino, B. Yan, S.G. Elci, E. Purdue, S. Goldring, F. Macaluso, N. Cobelli, R.W. Vachet, L. Santambrogio, Molecular analysis of chromium and cobalt-related toxicity, Sci. Rep. 4 (2014) 1–12. doi:10.1038/srep05729.

[2] S.M. Bradberry, J.M. Wilkinson, R.E. Ferner, Systemic toxicity related to metal hip prostheses, Clin. Toxicol. (Phila). 3650 (2014) 1–11. doi:10.3109/15563650.2014.944977.

[3] R.P. Wedeen, L. Qian, Chromium-induced kidney disease, Environ. Health Perspect. 92 (1991) 71–74.

[4] A.D. Dayan, A.J. Paine, Mechanisms of chromium toxicity, carcinogenicity and allergenicity: review of the literature from 1985 to 2000, Hum. Exp. Toxicol. 20 (2001) 439–451. doi:10.1191/096032701682693062.

[5] R. Yu, Cobalt toxicity, an overlooked cause of hypothyroidism, J Endocrinol Thyroid Res. 1 (2017) 1–4.

[6] S. Moniz, S. Hodgkinson, P. Yates, Cardiac transplant due to metal toxicity associated with hip arthroplasty, Arthroplast. Today. (2017) 4–6. doi:10.1016/j.artd.2017.01.005.

[7] C.J. Gilbert, A. Cheung, J. Butany, M.G. Zywiel, K. Syed, M. McDonald, F. Wong, C. Overgaard, Hip pain and heart failure: The missing link, Can. J. Cardiol. 29 (2013) 639.e1-639.e2. doi:10.1016/j.cjca.2012.10.015.

[8] C.A. Moran, F.G. Mullick, K.G. Ishak, F.B. Johnson, W.B. Hummer, Identification of titanium in human tissues: Probable role in pathologic processes, Hum. Pathol. 22 (1991) 450–454. doi:10.1016/0046-8177(91)90130-H.

[9] Y. Cui, X. Gong, Y. Duan, N. Li, R. Hu, H. Liu, M. Hong, M. Zhou, L. Wang, H. Wang, F. Hong, Hepatocyte apoptosis and its molecular mechanisms in mice caused by titanium dioxide nanoparticles, 183 (2010) 874–880. doi:10.1016/j.jhazmat.2010.07.109.

[10] L. Sheng, X. Wang, X. Sang, Y. Ze, X. Zhao, D. Liu, S. Gui, Q. Sun, J. Cheng, Z. Cheng, R. Hu, L. Wang, F. Hong, Cardiac oxidative damage in mice following exposure to nanoparticulate titanium dioxide, J. Biomed. Mater. Res. - Part A. 101 (2013) 3238–3246. doi:10.1002/jbm.a.34634.

[11] M. Costa, Toxicity and carcinogenicity of Cr(VI) in animal models and humans, Crit. Rev. Toxicol. 27 (1997) 431–442. doi:10.3109/10408449709078442.
[12] M.G. Shettlemore, K.J. Bundy, Examination of in vivo influences on bioluminescent microbial assessment of corrosion product toxicity, Biomaterials. 22 (2001) 2215–2228. doi:10.1016/S0142-9612(00)00410-5.
[13] K. Merritt, S.A. Brown, Release of hexavalent chromium from corrosion of stainless steel and cobalt—chromium alloys, J. Biomed. Mater. Res. 29 (1995) 627–633. doi:10.1002/jbm.820290510.
[14] Y. Hedberg, I.O. Wallinder, Metal release and speciation of released chromium from a biomedical CoCrMo alloy into simulated physiologically relevant solutions, J. Biomed. Mater. Res. - Part B Appl. Biomater. 102B (2014) 693–699. doi:10.1002/jbm.b.33048.
[15] M. Haeri, W. Torsten, G.M. Langford, J.L. Gilbert, Biomaterials Electrochemical control of cell death by reduction-induced intrinsic apoptosis and oxidation-induced necrosis on CoCrMo alloy in vitro, Biomaterials. 33 (2012) 6295–6304. doi:10.1016/j.biomaterials.2012.05.054.
[16] A.J. Hart, P.D. Quinn, F. Lali, B. Sampson, J.A. Skinner, J.J. Powell, J. Nolan, K. Tucker, S. Donell, A. Flanagan, J.F.W. Mosselmans, Cobalt from metal-on-metal hip replacements may be the clinically relevant active agent responsible for periprosthetic tissue reactions, Acta Biomater. 8 (2012) 3865–3873. doi:10.1016/j.actbio.2012.05.003.
[17] A. Di Laura, P.D. Quinn, V.C. Panagiotopoulou, H.S. Hothi, J.J. Powell, F. Berisha, F. Amary, J.F.W. Mosselmans, J.A. Skinner, A.J. Hart, The Chemical Form of Metal Species Released from Corroded Taper Junctions of Hip Implants : Synchrotron Analysis of Patient Tissue, Sci. Rep. 7 (2017) 1–13. doi:10.1038/s41598-017-11225-w.
[18] R.M. Urban, J.J. Jacobs, M.J. Tomlinson, J. Gavrilovic, J. Black, M. Peoc'h, Dissemination of wear particles to the liver, spleen, and abdominal lymph nodes of patients with hip or knee replacement, J. Bone Joint Surg. Am. 82–A (2000) 457–476. http://www.ncbi.nlm.nih.gov/pubmed/10761937.
[19] P. Campbell, R. Urban, I. Catelas, A. Skipor, T. Schmalzried, Autopsy analysis thirty years after metal-on-metal total hip replacement, J. Bone Jt. Surg. 85 (2003) 2218–2222.
[20] C.P. Case, V.G. Langkamer, C. James, M.R. Palmer, A.J. Kemp, P.F. Heap, L. Solomon, Widespread dissemination of metal debris from implants, J. Bone Jt. Surgery. 76 (1994) 701–12. http://www.ncbi.nlm.nih.gov/pubmed/8083255.
[21] R. Michel, M. Noite, M. Reich, Systemic effects of implanted prostheses made of cobalt-chromium alloys, Arch. Orthop. Trauma Surg. 110 (1991) 61–74.
[22] A. Abdel-Gadir, R. Berber, J.B. Porter, P.D. Quinn, D. Suri, P. Kellman, A.J. Hart, J.C. Moon, C. Manisty, J.A. Skinner, Detection of metallic cobalt and chromium liver deposition following failed hip replacement using T2* and R2 magnetic resonance, J. Cardiovasc. Magn. Reson. 18 (2016) 29. doi:10.1186/s12968-016-0248-z.
[23] P.L. Day, S.J. Eckdahl, J.J. Maleszewski, T.C. Wright, D.L. Murray, Establishing human heart chromium, cobalt and vanadium concentrations by inductively coupled plasma mass spectrometry, J. Trace Elem. Med. Biol. 41 (2017) 60–65. doi:10.1016/j.jtemb.2017.02.009.
[24] J.F.W. Mosselmans, P.D. Quinn, A.J. Dent, S.A. Cavill, S.D. Moreno, A. Peach, P.J. Leicester, S.J. Keylock, S.R. Gregory, K.D. Atkinson, J.R. Rosell, I18 - The microfocus spectroscopy beamline at the Diamond Light Source, J. Synchrotron Radiat. 16 (2009) 818–824. doi:10.1107/S0909049509032282.

[25] V.A. Solé, E. Papillon, M. Cotte, P. Walter, J. Susini, A multiplatform code for the analysis of energy-dispersive X-ray fluorescence spectra, Spectrochim. Acta - Part B At. Spectrosc. 62 (2007) 63–68. doi:10.1016/j.sab.2006.12.002.
[26] B. Ravel, M. Newville, ATHENA, ARTEMIS, HEPHAESTUS: Data analysis for X-ray absorption spectroscopy using IFEFFIT, J. Synchrotron Radiat. 12 (2005) 537–541. doi:10.1107/S0909049505012719.
[27] C.C. Wyles, T.C. Wright, M.C. Bois, M.S. Amin, A. Fayyaz, S.M. Jenkins, S.P. Wyles, P.L. Day, D.L. Murray, R.T. Trousdale, N.S. Anavekar, W.D. Edwards, J.J. Maleszewski, Myocardial cobalt levels are elevated in the setting of total hip arthroplasty, J. Bone Joint Surg. Am. 99 (2017) e118. doi:10.2106/JBJS.17.00159.
[28] A.J. Hart, P.D. Quinn, B. Sampson, A. Sandison, K.D. Atkinson, J.A. Skinner, J.J. Powell, J.F.W. Mosselmans, The chemical form of metallic debris in tissues surrounding metal-on-metal hips with unexplained failure, Acta Biomater. 6 (2010) 4439–4446. doi:10.1016/j.actbio.2010.06.006.
[29] R.M. Urban, M.J. Tomlinson, D.J. Hall, J.J. Jacobs, Accumulation in liver and spleen of metal particles generated at nonbearing surfaces in hip arthroplasty, J. Arthroplasty. 19 (2004) 94–101. doi:10.1016/j.arth.2004.09.013.
[30] M. Huber, G. Reinisch, G. Trettenhahn, K. Zweymüller, F. Lintner, Presence of corrosion products and hypersensitivity-associated reactions in periprosthetic tissue after aseptic loosening of total hip replacements with metal bearing surfaces, Acta Biomater. 5 (2009) 172–180. doi:10.1016/j.actbio.2008.07.032.
[31] R.M. Urban, J.J. Jacobs, Migration of corrosion products from modular hip prostheses. Particle microanalysis and histopathological findings, J. Bone Jt. Surg. Am. 76 (1994) 1345.
[32] A.J. Hart, A. Sandison, P. Quinn, B. Sampson, K.D. Atkinson, J. a Skinner, A. Goode, J.J. Powell, J.F.W. Mosselmans, Microfocus study of metal distribution and speciation in tissue extracted from revised metal on metal hip implants, J. Phys. Conf. Ser. 190 (2009) 1–5. doi:10.1088/1742-6596/190/1/012208.
[33] A.W.E. Hodgson, S. Kurz, S. Virtanen, V. Fervel, C.O.A. Olsson, S. Mischler, Passive and transpassive behaviour of CoCrMo in simulated biological solutions, Electrochim. Acta. 49 (2004) 2167–2178. doi:10.1016/j.electacta.2003.12.043.
[34] R.B. Hayes, The carcinogenicity of metals in humans, Cancer Causes Control. 8 (1997) 371–385. doi:10.1023/A:1018457305212.
[35] Chromium(VI) compounds-IARC Monographs on the Evaluation of Carcinogenic Risks to Humans, 100 C (2011) 147–167.
[36] I. Zadnipryany, O. Tretiakova, T. Sataieva, W. Zukow, Experimental review of cobalt induced cardiomyopathy, Russ. Open Med. J. 6 (2017) 1–4. doi:10.15275/rusomj.2017.0103.
[37] V.G. Langkamer, C.P. Case, P. Heap, A. Taylor, C. Collins, M. Pearse, L. Solomon, Systemic distribution of wear debris after hip replacement. A cause for concern?, J. Bone Joint Surg. Br. 74 (1992) 831–9. http://www.ncbi.nlm.nih.gov/pubmed/1447243.
[38] B.F. Shahgaldi, F.W. Heatley, A. Dewar, B. Corrin, In vivo corrosion of cobalt-chromium and titanium wear particles., J. Bone Joint Surg. Br. 77 (1995) 962–6. http://www.ncbi.nlm.nih.gov/pubmed/7593115.
[39] A. Weir, P. Westerhoff, L. Fabricius, K. Hristovski, N. Von Goetz, Titanium dioxide nanoparticles in food and personal care products, Environ. Sci. Technol. 46 (2012) 2242–2250. doi:10.1021/es204168d.
[40] J. Wang, G. Zhou, C. Chen, H. Yu, T. Wang, Y. Ma, G. Jia, Y. Gao, B. Li, J. Sun, Y. Li, F. Jiao, Y. Zhao, Z. Chai, Acute toxicity and biodistribution of different sized titanium dioxide particles in mice after oral administration, 168 (2007) 176–185.

doi:10.1016/j.toxlet.2006.12.001.
[41] L.E. Wu, A. Levina, H.H. Harris, Z. Cai, B. Lai, S. Vogt, D.E. James, P.A. Lay, Carcinogenic chromium(VI) compounds formed by intracellular oxidation of chromium(III) dietary supplements by adipocytes, Angew. Chemie - Int. Ed. 55 (2016) 1742–1745. doi:10.1002/anie.201509065.
[42] A. Levina, P.A. Lay, Solution structures of chromium(VI) complexes with glutathione and model thiols, Inorg. Chem. 43 (2004) 324–335. doi:10.1021/ic034901v.
[43] S. Bajt, S.B. Clark, S.R. Sutton, M.L. Rivers, J. V Smith, Synchrotron X-ray microprobe determination of chromate content using X-ray absorption near-edge Structure, Anal. Chem. 65 (1993) 1800–1804. doi:10.1021/ac00061a026.
[44] E. Strub, R. Plarre, M. Radtke, U. Reinholz, H. Riesemeier, U. Schoknecht, K. Urban, P. Jüngel, Determination of Cr(VI) in wood specimen: A XANES study at the Cr K edge, Nucl. Instruments Methods Phys. Res. Sect. B. 266 (2008) 2405–2407. doi:10.1016/j.nimb.2008.03.011.
[45] M.W. Kendig, A.J. Davenport, H.S. Isaacs, The mechanism of corrosion inhibition by chromate conversion coatings from x-ray absorption near edge spectroscopy (Xanes), Corros. Sci. 34 (1993) 41–49. doi:10.1016/0010-938X(93)90257-H.
[46] R. Bartholomäus, K. Harms, A. Levina, P.A. Lay, Synthesis and characterization of a chromium(V) cis-1,2-cyclohexanediolato complex: a model of reactive intermediates in chromium-induced cancers., Inorg. Chem. 51 (2012) 11238–11240. doi:10.1021/ic301900q.
[47] R. Codd, J.A. Irwin, P.A. Lay, Sialoglycoprotein and carbohydrate complexes in chromium toxicity, Curr. Opin. Chem. Biol. 7 (2003) 213–219. doi:10.1016/S1367-5931(03)00017-6.
[48] A. Levina, R. Codd, G.J. Foran, T.W. Hambley, T. Maschmeyer, A.F. Masters, P.A. Lay, X-ray absorption spectroscopic studies of chromium(V/IV/III)-2-Ethyl-2-hydroxybutanoato(2-/1-) complexes, Inorg. Chem. 43 (2004) 6208–6216. doi:10.1021/ic030239r.
[49] S. De Flora, A. Camoirano, M. Bagnasco, C. Bennicelli, G.E. Corbett, B.D. Kerger, Estimates of the chromium(VI) reducing capacity in human body compartments as a mechanism for attenuating its potential toxicity and carcinogenicity, Carcinogenesis. 18 (1997) 531–537. doi:10.1093/carcin/18.3.531.
[50] R. Codd, C.T. Dillon, A. Levina, P.A. Lay, Studies on the genotoxicity of chromium: from the test tube to the cell, Coord. Chem. Rev. 216–217 (2001) 537–582.
[51] K.M. Shah, P.D. Quinn, A. Gartland, J.M. Wilkinson, Understanding the tissue effects of tribo-corrosion: Uptake, distribution, and speciation of cobalt and chromium in human bone cells, J. Orthop. Res. 33 (2015) 114–121. doi:10.1002/jor.22729.
[52] B.J. Goldstein, K. Mahadev, X. Wu, L. Zhu, H. Motoshima, Role of insulin-induced reactive oxygen species in the insulin signaling pathway., Antioxid. Redox Signal. 7 (2005) 1021–31. doi:10.1089/ars.2005.7.1021.
[53] A. Levina, I. Mulyani, P.A. Lay, Redox chemistry and biological activities of chromium(III) complexes, The Nutritional Biochemistry of Chromium(III), Chapter 11 (2007) 223–255.
[54] I. Mulyani, A. Levina, P.A. Lay, Biomimetic oxidation of chromium(III): Does the antidiabetic activity of chromium(III) involve carcinogenic chromium(VI)?, Angew. Chemie - Int. Ed. 43 (2004) 4504–4507. doi:10.1002/anie.200460113.
[55] D.M. Niedowicz, D.L. Daleke, The role of oxidative stress in diabetic complications, Cell Biochem. Biophys. 43 (2005) 289–330. doi:10.1385/CBB:43:2:289.
[56] O. Addison, A.J. Davenport, R.J. Newport, S. Kalra, M. Monir, F.W. Mosselmans, D. Proops, R.A. Martin, Do “passive” medical titanium surfaces deteriorate in service in

the absence of wear?, J. R. Soc. Interface. 9 (2012) 3161–3164. doi:10.1098/rsif.2012.0438.
[57] P.J. Barnard, A. Levina, P.A. Lay, Chromium (V) peptide complexes: synthesis and spectroscopic characterization, Inorg. Chem. 44 (2005) 805–809.
[58] H.H. Harris, A. Levina, C.T. Dillon, P.A. Lay, Time-dependent uptake, distribution and biotransformation of chromium(VI) in individual and bulk human lung cells: application of synchrotron radiation techniques, J Biol Inorg Chem. 10 (2005) 105–118. doi:10.1007/s00775-004-0617-1.
[59] R. Tharani, F.J. Dorey, T.P. Schmalzried, The risk of cancer following total hip or knee arthroplasty, J. Bone Joint Surg. Am. 83–A (2001) 774–780.
[60] T. Visuri, E. Pukkala, P. Paavolainen, P. Pulkkinen, E.B. Riska, Cancer risk after metal on metal and polyethylene on metal total hip arthroplasty, Clin Orthop Relat Res. 4000 (1996) S280-289. doi:10.1097/00003086-199608001-00025.
[61] J. Sullivan, M. Parker and S.B. Carson, Tissue cobalt content in " beer drinkers " myocardiopathy, J Lab Clin Med. 71, 1968, 893-11.
[62] M. Barborik and J. Dusek, Cardiomyopathy accompanying industrial cobalt exposure, Br Heart J. 34, 1972, 113-6.
[63] J.R. Curtis, G.C.Goode, J. Herrington and L.E. Urdaneta, Possible cobalt toxicity in maintenance hemodialysis patients after treatment with cobaltous chloride: a study of blood and tissue cobalt concentrations in normal subjects and patients with terminal and renal failure, Clin Nephrol. 5, 1976, 61-5.
[64] I.H. Manifold, M.M Platts and A. Kennedy, Cobalt cardiomyopathy in a patient on maintenance haemodialysis, Br Med J. 2, 1978, 1609.
[65] A. Kennedy, J. Dornan and R. King, Fatal myocardial disease associated with industrial exposure to cobalt, The Lancet. 317, 1981, 412-14.
[66] L.A Allen, A.V. Ambardekar, K.M. Devaraj, J.J. Maleszewski and E.E. Wolfel, Clinical problem-solving. Missing elements of the history, N Engl J Med. 370, 2014, 559-66.
[67] J.R. Martin, L. Spencer-Gardner, C.L. Camp, J.M. Stulak and R.J. Sierra, Cardiac cobaltism: a rare complication after bilateral metal-on-metal total hip arthroplasty, Arthroplasty Today. 1, 2015, 99-102.
[68] K. Fox, T.M. Phillips, J.H. Yanta and M.G. Abesamis, Fatal cobalt toxicity after total hip arthroplasty revision for fractured ceramic components, 54, 2016, 874-77.

APPENDIX

Table A.1. Laser ablation operating parameters.

Wavelength	193 nm
Spot size	25-40 μm
Frequency	10 Hz
Scan speed	20 nm sec^{-1}
Energy	40-50%, 0.12 mJ
Helium flow rate	600 mL min^{-1}

Table A.2. Isotopes measured.

Ion	**Dwell time (ms)**
C^{13}	0.05
Si^{28}	0.02
P^{31}	0.2
Ca^{44}	0.02
Ti^{49}	0.25
Cr^{52}	0.2
Fe^{56}	0.2
Co^{59}	0.25
Cu^{63}	0.1
Zn^{64}	0.2

Table A.3. ICP-MS operating parameters.

Instrument settings	
Power	1250 W
Collision gas	Helium 2 mL min^{-1}
Nebuliser gas flow	1.0 L min^{-1}
Plasma gas flow	15 L min^{-1}

Table A.4. Cardiac Co load in exposed individuals and associated toxicity symptoms.

Reference	**Cardiac Co level** (ug/g)	**Source of metal**	**Result**
[61]	**0.48**[a]	Cobalt additive in beer combined with malnutrition.	Acute onset of left- and then right-sided heart failure with hypotension, pericardial effusion and progressive dyspnea; fatal cardiomyopathy.
[62]	**0.37** [a] **1.4**[b]	Occupational exposure to Co for 4 years.	Cardiomegaly with cobalt cardiomyopathy; death.
[63]	**1.65**[b]	3-month cobalt chloride therapy with hemodialysis.	Cardiomegaly with cobalt cardiomyopathy; death.
[64]	**8.9**	9-month cobalt chloride therapy with hemodialysis.	Cardiomegaly, pericardial effusion, poor LVEF, intractable biventricular failure; death.
[65]	**7**	Occupational exposure to Co powder for 4 years.	Changes consistent with cobalt cardiomyopathy.
[7]	**3.85**	Fracture of ceramic hip replacement followed by revision to a MoP prosthesis.	Pericardial effusion, dilated cardiomyopathy with global hypokinesis and EF of 30%; death.
[66]	**8.32**	Catastrophic wear of bilateral MoM hip replacement.	Pericardial effusion, low cardiac output with poor end-organ perfusion and a LVEF of 10%; heart transplantation.
[67]	**4.75**	Catastrophic wear of bilateral MoM hip replacement.	Severely abnormal right and left ventricular function with an EF of 10%-15%; dilated cobalt cardiomyopathy; death.
[68]	**2.5**	Fracture of ceramic hip replacement followed by revision to a MoP prosthesis.	Cardiomyopathy with global LV hypokinesis and an EF of 35–40%; death.
[23]	**3.756**[b]	Catastrophic wear of bilateral MoM hip replacement.	Progressive biventricular heart failure with an EF of 16%; death.
Current series (n=5)	**0.31-0.91**[b]	Wear and corrosion of metal components of joint implants.	Cardiomegaly (4/5 patients) and/or severe interstitial fibrosis (3/5 patients).

[a]ug/g wet tissue [b]ug/g dry tissue LVEF- left ventricular ejection fraction

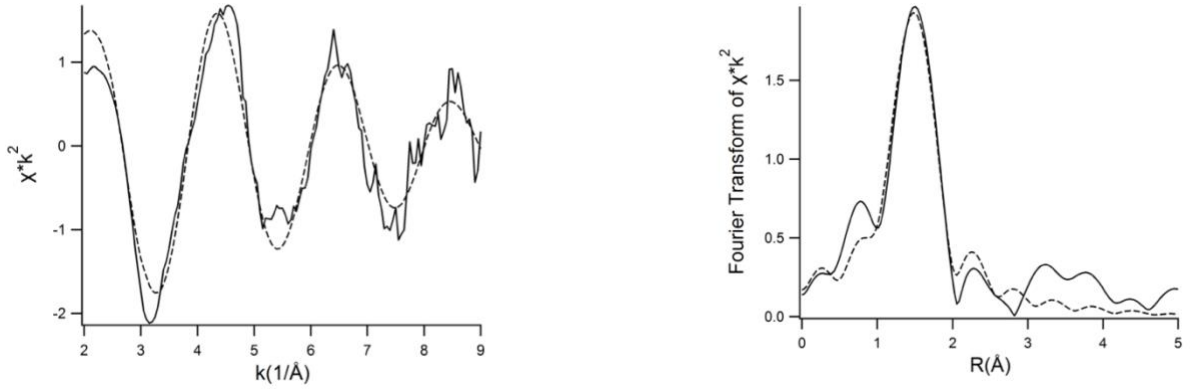

Sample	Path	Degeneracy	Distance (Å)	Debye Waller factor ($Å^2$)	R factor
Patient 1 spleen	Cr-O	6	1.97 (0.02)	0.0047 (0.002)	0.014

Figure A.1. Comparison of k^3-weighted EXAFS and Fourier transform spectra for Cr found in splenic tissue of Patient 1 (solid line) with that of $Cr(H_2O)_6$ (dashed line). EXAFS parameters for fit are included in the table.